Fine Structure of Short-Lived States of Hydrogen by a Microwave-Optical Method. II*

L. R. WILCOX† AND W. E. LAMB, JR.‡
Department of Physics, Stanford University, Stanford, California
(Received April 15, 1960)

This article describes improvements in the apparatus used in Part I by Lamb and Sanders to determine fine-structure separations in excited states $n=3$ and 4 of deuterium. Experimental and theoretical studies are made of the effects of environmental electric fields on the relative intensities of various resonances in order to obtain information about possible Stark shifts of the fine-structure levels. The density matrix method, used in Part I for two levels, is extended to N levels and is worked out more explicitly for the case of three levels. The splitting $3\,^2S_{\frac{1}{2}}-3\,^2P_{\frac{1}{2}}$ is found to be 315.30±0.80 Mc/sec compared with a calculated value of 315.34 Mc/sec. Less precise measurements are made for other separations which are also in good agreement with theory.

IN the preceding article[1] (denoted as Part I) a radio frequency-optical technique applicable to the study of hydrogenic fine structure has been described and preliminary results given. We report here on some improvements in the apparatus and further developments of the theory of the experiment. Accuracy of measurement of the $3s$-$3p$ splittings in deuterium has been considerably increased, and rough measurements were made of $3p$-$3d$ and $4s$-$4p$ separations.

A. MODIFICATIONS OF APPARATUS

A cross section of the main apparatus is shown in Fig. 1 and an "artist's" sketch in Fig. 2. The essential parts are (1) electron bombarder tube, (2) optical system, (3) rf system, and (4) a pair of Helmholtz coils. These component parts and auxiliary equipment will be described here only insofar as the differ from the equipment used in Part I.

1. Bombardment Tube

(a) *Design Changes*

The Mark V bombarder tube from which most of the data reported here were obtained was essentially an axially symmetric tetrode mounted in a 1.22-in. o.d. Nonex glass envelope (Fig. 3). Internal parts were constructed of molybdenum and tungsten in order to avoid magnetic disturbances. The oxide cathode was heated by passing approximately one ampere ac through the heater coil; the rms magnetic field at the interaction region arising from heater current did not exceed 10^{-2} gauss and could be neglected.

In the earlier versions of the bombardment tube the absence of a control grid hampered accurate and stable control of the beam current. The cathode surface was lanthanum boride. This cathode is relatively insensitive to "poisoning" by gaseous impurities, such as water vapor, and can be reactivated after exposure to the atmosphere. It was found that such ruggedness was unnecessary. Since lanthanum boride material emits at a much higher temperature than "oxide" cathode material, a substantial reduction of background light at the detector was obtained when lanthanum boride was replaced by "oxide". The slow absorption of deuterium gas by the oxide cathode seemed in no way to affect its thermionic emission.

(b) *Associated Components of the Vacuum Envelope*

As in earlier versions a Bayard-Alpert gauge (WL-5966) and a palladium tube were sealed on to the bombarder envelope. The ion gauge served mainly to indicate the rate of outgassing or leakage which continued after the assembly had been baked and sealed off before deuterium had been admitted through the heated palladium tube. After the bombardment tube had been filled to an operating pressure of from 1 to 10 microns, the ion gauge could not be conveniently used

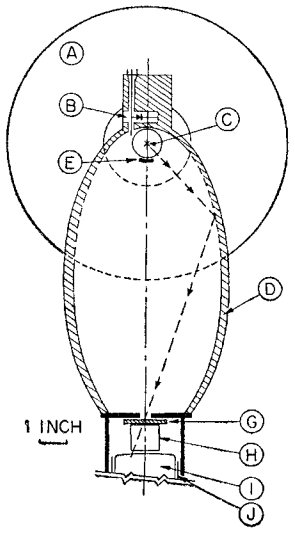

FIG. 1. Cross section of main apparatus. A. Helmholtz coil, B. rf probe, C. electron beam, D. elliptical mirror, E. rf electrode, G. interference filter, H. Lucite light pipe, I. photomultiplier, J. mu-metal shield.

* Work supported by the Office of Naval Research and based in part on a doctoral thesis by L. R. Wilcox, Stanford University, 1957.
† Present address: Gordon McKay Laboratory, Harvard University.
‡ Present address: Oxford University, Oxford, England.
[1] W. E. Lamb, Jr., and T. M. Sanders, Jr., preceding paper [Phys. Rev. 119, 1901 (1960)].

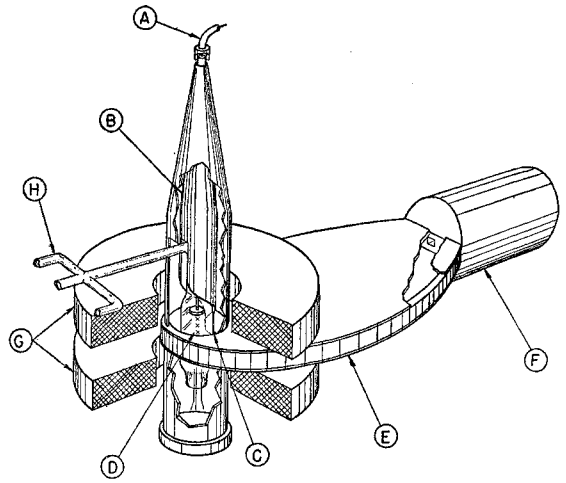

FIG. 2. Cutaway sketch of the main apparatus. A. rf input-50 ohm coaxial cable, B. rf tapered section, C. rf electrode, D. interaction region, E. elliptical mirror, F. light tight photomultiplier shield, G. Helmholtz coils, H. tubulation to ion gauge and *Pd* leak.

because of its powerful pumping action. When the tungsten filament was turned on the pressure dropped quickly by a factor of about 8. To make use of the ion gauge it would have been necessary to overfill the experimental tube by a large factor and to run the gauge continuously. Since it was easy to add deuterium to the tube but difficult to remove it through the palladium, the operating pressure was established with the ion gauge off. One then had a convenient recourse to the ion gauge if it was desired to lower the pressure. Preliminary measurements established that the Balmer-α light intensity from the bombarder was proportional to the pressure as measured by the ion gauge and from time to time a proportionality coefficient was established for a standard set of operating conditions. The pressure was monitored in this way, making minimal use of the ion gauge.

The failure to develop a satisfactory method for control and measurement of the hydrogen pressure had unfortunate consequences in our later work. It would be very desirable to repeat the measurements with a uranium hydride reservoir of hydrogen in the tube assembly.

2. Optical System

The optical system should serve to collect light emanating from, and only from, a cylindrical region about $\frac{3}{4}$ in. in length and $\frac{1}{4}$ in. in diameter in the drift space of the bombarder tube. It is necessary to have the photomultiplier detector well removed from the bomarder which is necessarily located in a strong magnetic field. Several schemes for guiding the light to the photomultiplier without serious loss of intensity were tried. This was best accomplished with a mirror in the form of an elliptic cylinder (Fig. 1). The bombarder beam was centered on one focal line of a silvered elliptical cylinder while the other focus, 10 in. removed, was located at an exit aperture leading to the detector. The mirror, though crude by usual optical standards, produced a tenfold increase in collected flux over the previously used lens system, and was superior to a Lucite light pipe in its ability to reject extraneous background light.

3. Rf System

(*a*) *Coaxial Geometry*

Changes in the rf system were necessitated by the changes in the optical system described above. In order to stimulate the desired σ-type transitions, there should be an rf electric field component perpendicular to the tube axis. The means by which the rf field was applied to the interaction region are illustrated in Figs. 2 and 3. It can be seen from these figures that in some approximations the metallic projection extending downward from the large center conductor tends to place the bombardment region between the conductors of a roughly plane parallel transmission line, the wall of the elliptical mirror being the other conductor. Mainly because of the proximity of the anode and grid structures the fringing fields were rather large and both σ- and π-type transitions could be observed with our apparatus.

The wide range of frequencies over which transitions were studied (300–3700 Mc/sec) dictated the use of the

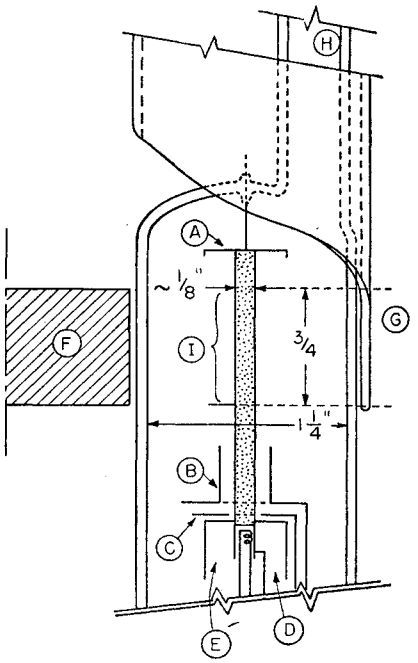

FIG. 3. Cross section of *Mk V* bombardment tube showing electrodes. A. collector electrode, B. light baffle and accelerator grid, C. control grid, D. heat and light shield, E. oxide cathode, F. back end of elliptical cylinder serving as rf ground electrode, G. extension of rf coaxial conductor, H. tubulation to ion gauge and *Pd* leak, I. interaction region.

coaxial transmission mode. Since power requirements were modest (milliwatts), a high Q resonant structure was neither necessary nor desirable. On the other hand, for a given set of runs, the frequency was kept constant and a well matched, broad-band structure was not required. In an attempt to avoid troublesome resonances in the apparatus, the transition from 50-ohm coaxial cable to the larger quasi-coaxial geometry of the apparatus was made somewhat smoothly in the tapered section shown in Fig. 2.

(b) *Rf Probe*

Relative measurements of the rf electric field strength in close proximity to the interaction region could be made with the capacitive probe and crystal assembly shown in Fig. 1. After verification of proper "square law" operation of the crystal one could relate the crystal current to the absolute rf electric field strength by observing the degree of saturation of a fine-structure resonance (See Sec. 11). The probe sensitivity was found to be highly dependent on frequency, making a recalibration necessary at each frequency used. The voltage output of the probe was monitored on an oscilloscope to ensure correct and stable modulation of the rf source.

(c) *Rf Sources*

To improve its stability, the WL 417A klystron used in these experiments was placed in a water-cooled oil bath. A fixed 10 db broad-band attenuator and a variable 1–20 db Sanders "tri-plate" attenuator provided padding and control of the rf amplitude.

For measurements of an exploratory nature in the frequency range 2400–2900 Mc/sec a Sylvania 6BL6 klystron with external cavity served well. In the range from 250–2000 Mc/sec, two General Radio oscillators (1209B and 1218A) were used.

TABLE I. Values of unit electric fields defined in Eq. (1) for all possible $n=3$ transitions. These are calculated assuming that J is a good quantum number.

Transitions	Unit field (volt/cm)
σ transitions	
$a\alpha$ $d\beta$	0.41
αf βe	0.50
$b\beta$ $c\alpha$	0.71
Aa Fd	1.50
Ge Jf	1.65
Bb Ec	1.94
Cc bD	2.75
Hf Ie	2.86
Dd Ca	4.76
bI cH	5.05
aH dI	5.84
cJ bG	5.84
π transitions	
$c\beta$ $b\alpha$	0.35
αe βf	0.50
Dc Cb	1.37
He If	1.42
Ed Ba	1.68
aG dJ	3.37
bH cI	10.10

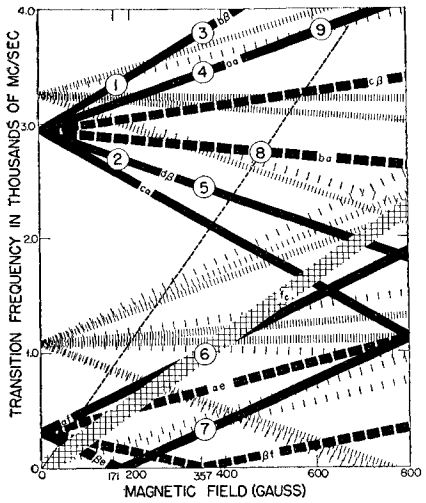

FIG. 4. Level differences for transitions of interest. Relative strength is indicated by density of shading. The numerals in circles refer to regions where some complicating phenomena can be present.

4. Magnet

(a) *Field Homogeneity*

The Helmholtz coils and associated regulated power supply were taken over from the earlier experiments but considerable improvement in field homogeneity was obtained by further adjustment of the coil spacing. From our measurements it was concluded that the limits of field variation over the sensitive volume was ± 100 ppm which resulted in negligible line-broadening and distortion.

(b) *Magnet Calibration*

Magnetic fields in the Helmholtz coil were inferred from measurements of the coil current. Calibration points were established with a proton resonance apparatus toward the beginning of the experimental period, and again near the conclusion. These calibrations were consistent to within 100 ppm.

There was a systematic variation of magnet calibration with magnet current. After moving from one field to another, the calibration "constant" was observed to drift for about an hour. With sufficient time allowed, the effect amounted to 800 ppm over the working range of magnet currents, and was presumably caused by thermal and elastic deformation of the coils and coil spacing. Since these effects are both proportional to the square of the magnet current, calibration points at several field strengths were fitted to a formula of the form $H=(a-bV^2)V-H_e$. Here V is a voltage proportional to the magnet current and $H_e=0.3$ gauss is a contribution from the vertical component of the earth's field.

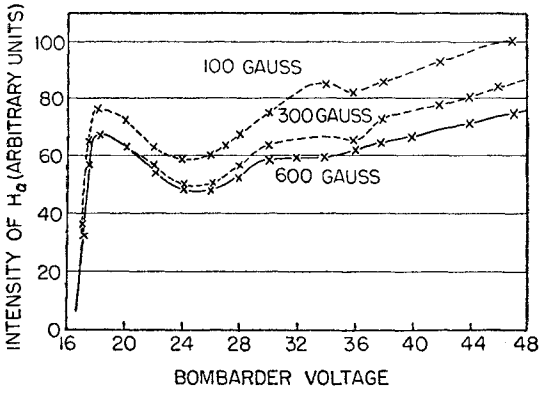

FIG. 5. Intensity of Balmer α light vs beam energy in various magnetic fields.

With this more elaborate field calibration we conclude that the uncertainty in magnetic field does not exceed ± 200 ppm with an additional uncertainty of ± 0.1 gauss coming from possible variations of H_e in our laboratory. Errors which might arise from these uncertainties are small compared to those from other sources.

B. FINE-STRUCTURE RESONANCES

6. Choice of Transitions

Table III of Part I gives matrix elements $(\mu|\mathbf{r}|\nu)$ for all possible electric dipole transitions between the $n=3$ states of hydrogen. It is convenient to define "unit fields" $\mathcal{E}_{\mu\nu}$ such that when the rf amplitude $\mathcal{E}_{\mathrm{rf}}=2\mathcal{E}_{\mu\nu}$ the transition $\nu\rightarrow\mu$ is 50% saturated (See Part I, Sec. 1). With the radiative decay constants denoted by γ, these fields are given by

$$\mathcal{E}_{\mu\nu}=\tfrac{1}{2}(300\hbar/e)(\gamma_\mu\gamma_\nu)^{\frac{1}{2}}/|(\mu|\mathbf{r}|\nu)| \qquad (1)$$

in volt/cm and are evaluated numerically in Table I.

Zeeman energy differences associated with the fine structure of $n=3$ states are shown in Fig. 4. All possible σ-type transitions (rf electric field normal to the fixed magnetic field) and the four strongest π-type transitions are shown (heavy dashed lines). Some attempt has been made in the figure to indicate relative intensities as well as natural linewidths in order to show the degree of expected overlapping. The cross-hatched diagonal band locates the electron cyclotron resonance which prevents fine structure measurements in or near the band. The dotted curve corresponds to twice the cyclotron frequency. Such harmonic resonances, although much weaker than the cyclotron resonances, could be clearly seen. They can occur in a nonuniform rf field in which the electron's orbital motion introduces new frequencies into the rf force acting on it.

For reasons mentioned in Part I the $a\alpha$ transitions are found to yield the most precise results for the electromagnetic shift $\mathbb{S}$, but a number of other transitions were studied with a view toward increasing the understanding of possible sources of error and for whatever incidental light they might shed upon atomic processes.

C. OPERATING CHARACTERISTICS

7. Bombarder Tube

(a) *Behavior in Zero Magnetic Field*

Because of wall and space-charge effects in our experimental tubes, a suitable electron beam could not be formed in the absence of an axial magnetic field. With hydrogen pressure at a few microns a 100-μa electron beam of, say, 25 volts energy manifested itself visibly by diffuse cones of light located near the accelerator and collector electrodes, while the intervening drift space region remained dark. Evidently, primary beam electrons were scattered by the gas to the glass walls of the tube envelope, driving them toward cathode potential, depressing the potential in the drift region and causing the beam energy to drop below the optical excitation threshold. When the accelerator voltage was increased to about 50 volts, a diffuse cylindrical beam sometimes appeared, depending on pressure. Evidently, positive ions were then formed at a rate sufficient to neutralize the negative wall charge.

(b) *Behavior in a Magnetic Field*

Suppose the beam voltage was above threshold, but the drift space was dark as described above. When an axial magnetic field of from 15 to 30 gauss was applied, a glowing cylindrical beam suddenly formed. The magnetic field at which this occurred depended upon gas pressure, beam voltage and current and was lower when any of these parameters was raised. The critical field corresponded roughly to that required to keep singly scattered beam electrons from reaching the walls.

(c) *Excitation Curves*

Figure 5 shows how the intensity of Balmer α light from the bombarder varied with beam voltage for several values of magnetic field. The appearance potential for H_α light, extrapolated to zero beam current, was close to the expected value of 16.6 ev. One might imagine that the rise occurring near 26 ev corresponded to the production of "fast" excited atoms discussed in

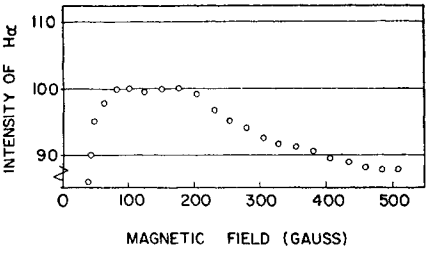

FIG. 6. Dependence of H_α light intensity on magnetic field for fixed beam voltage.

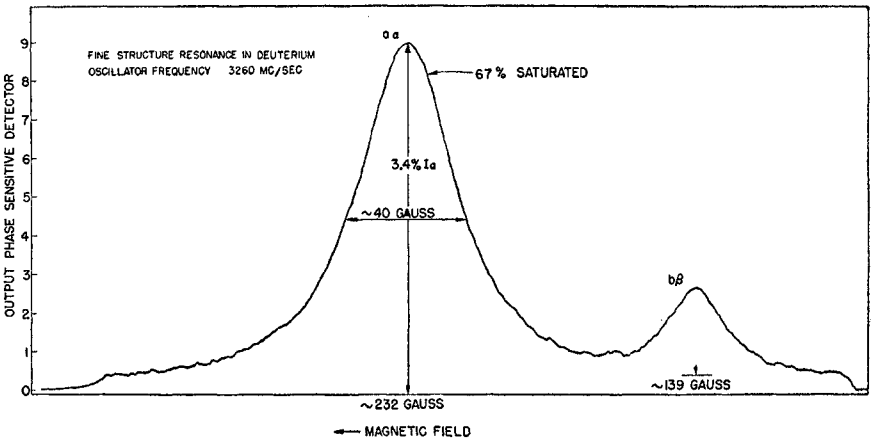

FIG. 7. Recorder trace, showing the $a\alpha$ and $b\beta$ resonances. The $b\beta$ resonance is partially quenched.

Part I, Sec. 10. This second threshold also showed up quite clearly in the excitation curves for the $a\alpha$ resonance. If the 26-ev "threshold" is associated with the appearance of energetic atoms, it seems likely that even at 50-ev beam energy the excitation of "fast" atoms does not exceed that of the slow ones.

In Fig. 6 it will be seen that for a given bombarding energy the H_α light intensity varied by about 11% over the useful range of magnetic fields from 90–500 gauss. Below 70 gauss, the dependence on field was too rapid to permit undistorted observation of fine structure resonances. There are many possible explanations for dependence of light output on magnetic field, but distortion of our resonance curves from such a variation was not serious in the present experiment.

8. Fine Structure Resonances

(a) *Strength of Resonances*

Figure 7 is a recorder trace, taken at 3260 Mc/sec, showing the two most important resonances for our work: $a\alpha$ and $b\beta$. It was found that the $a\alpha$ resonance maximum in Fig. 7 corresponded to a 3.4% change in the intensity of H_α light. From its width, one can infer that the resonance had 67% of its saturated height, so that the maximum obtainable signal (at large rf power) should be 5.1%. This is to be compared with the theoretical estimate of 6.5% based on assumption of equal excitation rates for all $n=3$ sublevels. The agreement is satisfactory in view of the uncertain validity of such an assumption.

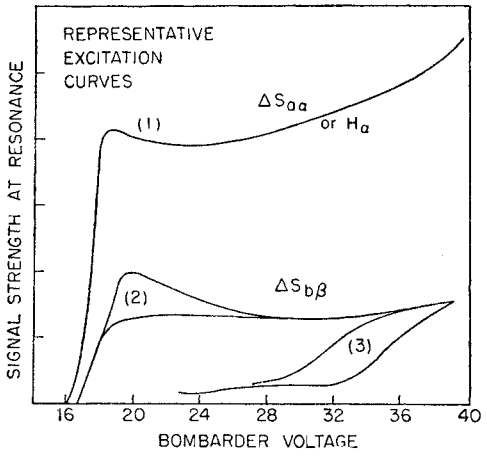

FIG. 8. Typical excitation curves. The appearance potential for H_α light is near 16 volts. Curves (2) and (3) were characteristic of high- and low-pressure respectively. At low pressure a hysteresis effect was observed.

(b) *Anomalies in Resonance Strength*

The squared matrix elements for the transitions $a\alpha$ and $b\beta$ shown in Fig. 7 are approximately in the ratio[2] 3:1. Assuming equal steady state populations of the α and β states in the absence of rf, the signal intensities should stand in the same 3:1 ratio for vanishingly small rf power, and should approach equality for large rf power. In the intermediate case shown in Fig. 7, the $a\alpha$ resonance is appreciably power broadened (by a factor $B=1.7$). A simple calculation based upon Eq. (6) of Part I indicates that the intensity ratio should be $(1+2B^{-2})=1.7$, but the observed ratio is more nearly 4. We are led to infer that the β state, and hence the $b\beta$ resonance, is differentially quenched by some mechanism. This is further discussed in Chapter D.

(c) *Excitation Curves for Resonances*

In Fig. 8 the typical dependence of resonance maxima upon bombarder beam voltage is shown. Details of the excitation curve vary with gas pressure, magnetic field, beam current, etc., but at low gas pressure it is found that the H_α intensity and the strength of the $a\alpha$ resonance are closely proportional. In contrast, excitation curves for the $b\beta$ resonance tended to be erratic and difficult to reproduce. Curves similar to (1) or (2) were the rule and curves such as (3), with or without hys-

[2] If J is not a good quantum number this ratio departs from 3:1. At the magnetic fields used in this work the error is small and we neglect it.

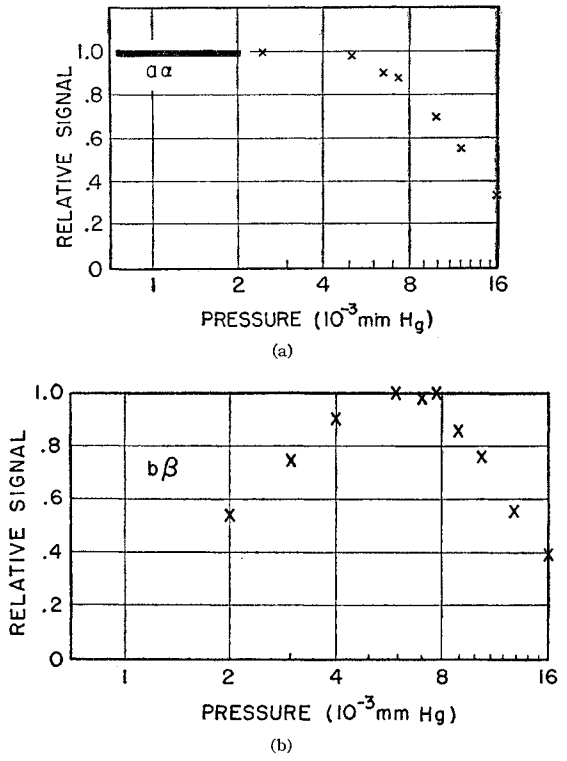

FIG. 9. (a) Signal strength vs pressure for $a\alpha$ resonance; (b) Signal strength vs pressure for $b\beta$ resonance. The signal is normalized by dividing by the total H_α intensity at each pressure. The weakening of $b\beta$ at low pressure is attributed to space-charge fields which increase as the density of neutralizing ions declines. Quenching at high pressure is attributed to ion "collisions."

teresis, presaged a "bad" condition. This "bad" condition was identified rather late in our work as one which could occur only when the gas pressure in the tube had fallen below a few microns. In Appendix III arguments are given that this phenomenon is caused by space charge of the electron beam.

(d) *Abnormal Line Center Shifts*

Measurements of line centers, made under conditions described above as "bad" were found to yield values for the level shift $3\,^2S_{\frac{1}{2}}-3\,^3P_{\frac{1}{2}}$ which differed by several Mc/sec from our usual results and from the theoretical value. The shifts encountered were always larger at low-beam energy. This correlates with curve (3) of Fig. 8 where a large "quenching" effect of $b\beta$, is found at low-beam energy.

(e) *Quenching at High Pressure*

For gas pressures above 8 microns, a second kind of quenching effect was observed. The $a\alpha$ and $b\beta$ resonances were both weakened with increasing pressure [See Fig. 9(a), (b)]. Other measurements show that this second kind of quenching is not dependent upon pressure alone, but upon beam current and energy as well, being reduced at low current and voltage. Further evidence that the α state was quenched at high pressure was obtained from studies of the dependence of the $a\alpha$ resonance maximum upon rf power. The power p_0 required for 50% saturation was measured at several pressures, keeping other tube parameters constant. The results are given in Table II and showed that p_0 increased with pressure. This is rather clear evidence that the lifetime of the α state is being reduced at high pressure.

The dependence upon pressure, beam current and voltage of the high-pressure quenching suggests that it may be attributed to positive ions in the bombardment tube. Estimates bearing on this hypothesis will be made in Appendix III.

D. ELECTRIC PERTURBATIONS

9. Need for Theory

As indicated in the preceding section, it was discovered that rather large variations in resonance signal and line center could occur as conditions changed within the experimental tube. The common cause for these effects is quite clearly traceable to perturbing electric fields. In this experiment, unlike that of Lamb and Retherford, the excited atoms are necessarily studied in the bombardment region, which is far from being a simple electrical environment. Possible sources of electric perturbations which act on the excited atoms are: (1) space charge within the electron beam, (2) charges on the glass walls or on insulating deposits within the apparatus, (3) motion of the excited atoms across the magnetic field, and (4) fluctuating fields resulting from nearby ions and electrons. As a further complication, fields from (1) and (2) are subject to ion neutralization depending on gas pressure, beam energy, etc.

The sensitivity of hydrogen-like atoms to electric perturbations increases very rapidly with increasing principal quantum number n and decreasing nuclear charge. In the experiment of Lamb and Skinner ($n=2$, $Z=2$), for example, the Stark shift for a given electric field is typically smaller by a factor of approximately 400 than in our case ($n=3$, $Z=1$). Thus perturbing effects in the bombardment region which were negligible in the ionized helium case are important in our case, limiting accuracy and complicating the interpretation of our resonances. It is, therefore, necessary to

TABLE II. Variation with pressure of power p_0 required for 50% saturation of $a\alpha$ resonance.

Pressure (microns)	Power p_0 (relative values)
3.9	1.0
5.0	1.0
8.0	1.3
13.6	2.2

enter upon a discussion of the perturbing effects of static or quasi-static electric fields. Speculations about the nature of these fields are given in Appendix III.

10. Three-Level Problem

We are concerned with excited states such as the $3s$ and $3p$ states of the hydrogen atom which decay by spontaneous emission. For such states the familiar treatment of Stark effect by time independent perturbation theory must be modified and supplemented. To do this we consider a problem involving the three decaying levels 1, 2, and 3 shown in Fig. 10.

Electric dipole matrix elements are assumed to exist between states 1 and 3 and between states 2 and 3, but not between 1 and 2. A radio frequency field $\mathcal{E}_{rf}\cos\nu t$ is responsible for the transitions between states 1 and 3, while an electrostatic field $\mathcal{E}_{es}$ couples 2 and 3. Let these states be excited at rates r_j, $j=1, 2, 3$ atoms per second, by the electron bombardment. Their decay through spontaneous transitions to lower atomic states is described as in Part I, Sec. 1, by phenomenological damping coefficients γ_j, $j=1, 2, 3$. The emission of H_α radiation occurs with branching ratios f_j which may be less than unity when other modes of de-excitation are present. The simpler problem which results if $\mathcal{E}_{es}$ vanishes has been treated in Part I, Sec. 1. We wish to learn how those results are modified by the second coupling field.

The general formalism which we have developed for treatment of this problem is explained in Appendix I. Use is made of the "population" matrix introduced in Part I, and the "Boltzmann" equation derived there is generalized to the case of arbitrarily many levels subject to many perturbations. It is shown that under certain conditions one may re-express the full quantum mechanical problem by means of a set of "rate" equations involving only diagonal elements of the population matrix, i.e., the steady-state populations. Further detailed analysis of the "three-level problem" will be found in Appendix II. The main results of that treatment are summarized below.

(a) *Rate Equations*

It is shown that the steady-state populations $n_j (j=1, 2, 3)$ satisfy a set of inhomogeneous linear equations

$$\dot{n}_j=-\gamma_j n_j+\sum_{k\neq j} W_{jk}n_k-n_j\sum_{k\neq j} W_{kj}+r_j. \qquad (2)$$

Because of their form, we shall call these "rate" equations, even though they hold rigorously only in the steady state when the $\dot{n}_j$ are zero.

(b) *Rate Constants*

The coefficients W_{ij} for the problem described above belong to a symmetric matrix W and only the three quantities W_{ij} for $i<j$ need be considered. These

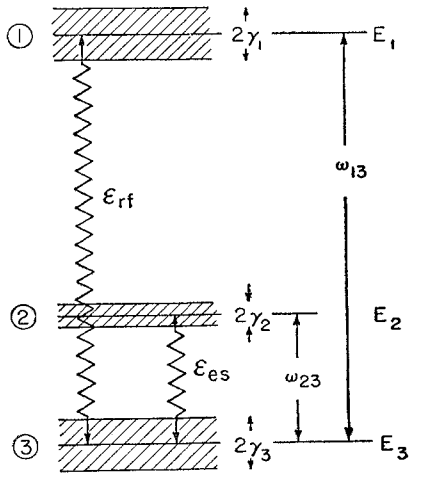

FIG. 10. The problem of three levels coupled by two perturbations.

depend on the energy splittings, decay rates and perturbing field strengths in a complicated way. Fortunately, for application to the problem at hand, a number of simplifying approximations are justified. In the lowest approximation, i.e., for small perturbations $\mathcal{E}_{rs}$ and $\mathcal{E}_{es}$, we find

$$\begin{aligned} W_{13}&=\Gamma_1(\mathcal{E}_{rf}/2\mathcal{E}_{13})^2\mathfrak{L}[(\omega_{13}-\nu)/\Gamma_2],\\ W_{23}&=\Gamma_1(\mathcal{E}_{es}/\mathcal{E}_{23})^2\mathfrak{L}[\omega_{23}/\Gamma_2], \qquad (3)\\ W_{12}&=0, \end{aligned}$$

with

$$\begin{aligned} \Gamma_1&=\gamma_s\gamma_p/(\gamma_s+\gamma_p),\\ \Gamma_2&=\tfrac{1}{2}(\gamma_s+\gamma_p), \qquad (4) \end{aligned}$$

and where the unit fields $\mathcal{E}_{\mu\nu}$ given by Eq. (1) are listed in Table I. The Lorentzian factors standing in Eq. (3) are abbreviated by the symbol

$$\mathfrak{L}[\theta]=1/(1+\theta^2). \qquad (5)$$

Comparison with Part I, Eq. (5) shows that our first approximation to W_{13} agrees, as it should, with the result obtained there for the case of two levels. In the lowest approximation for small $\mathcal{E}_{es}$, the only new effect is the occurrence of transitions between states 2 and 3.

Further expansion in powers of V yields effects which may be interpreted in terms of the Stark shift and quenching of the decaying states. The resonance shape is still Lorentzian but with shifted center, reduced height and increased width. In this approximation

$$W_{13}=\Gamma_1(\mathcal{E}_{rf}/2\mathcal{E}_{13})^2\mathfrak{L}[(\omega_{13}+\delta\omega_{13}-\nu)/(\Gamma_2+\delta\gamma_{13})], \qquad (6)$$

where

$$\delta\omega_{13}=\tfrac{1}{2}\Gamma_1(\mathcal{E}_{es}/\mathcal{E}_{23})^2(\omega_{23}/\Gamma_2)\mathfrak{L}[\omega_{23}/\Gamma_2], \qquad (7)$$

and

$$\delta\gamma_{13}=\tfrac{1}{4}\Gamma_1(\mathcal{E}_{es}/\mathcal{E}_{23})^2\mathfrak{L}[\omega_{23}/\Gamma_2]. \qquad (8)$$

In these formulas it is assumed that state 3 is an s state.

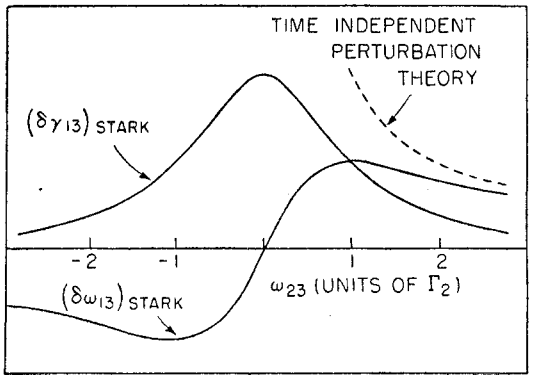

FIG. 11. Stark shift and broadening for decaying states near a crossing point.

When levels 2 and 3 are separated by many radiation widths, the shift becomes

$$\delta\omega_{13} \longrightarrow V^2/\omega_{23}, \tag{9}$$

which is the familiar result of time independent perturbation theory. In general, the "Stark" shift is always less than that predicted by the simpler theory, as shown in Fig. 11. A similar effect was noted in the work of Lamb and Retherford.[3]

(c) *Forbidden Transitions*

If $W_{12}\neq 0$, transitions between states 1 and 2 occur. Since there is no perturbing matrix element directly connecting states 1 and 2, these might be called forbidden transitions. The first nonvanishing contribution to W_{12} is of order $\mathcal{E}_{\rm rf}^2\mathcal{E}_{\rm es}^2$. A resonance related to W_{12} was found by Lamb and Retherford[4] to occur between the metastable $2\,^2S_{\frac{1}{2}}$ states α and β near the crossing point of β and e. In that case the states which we have called 1 and 2 are to be associated with long-lived s states, and our theory predicts that W_{12} may become large, i.e., comparable to W_{13} and W_{23}. Unfortunately, the analogous resonance for the present experiment is obscured by the strong and broad cyclotron resonance. We are therefore interested primarily in the case that states 1 and 2 are p states where W_{12} is negligibly small.

(d) *Solution of the "Rate" Equations*

Having obtained a set of rate equations and supposing the constants W_{ij} are known, it remains to solve for the steady-state populations and to calculate the rate of H_α emission from the ensemble. To obtain the quantity of direct experimental interest we must calculate this rate twice; first with both rf and electrostatic perturbations, and then with only the electrostatic perturbation. The difference in H_α intensities corresponds to the square wave rf amplitude modulation and gives the observed signal.

One can obtain a nearly complete idea of what happens by considering a simplified situation. Suppose the $3p$ states were so little excited in comparison with $3s$ that they contributed no H_α light. We would write Eq. (2) as

$$\dot{n}_s=0=-\gamma_s n_s-W_{\rm es}n_s-W_{\rm rf}n_s+r_s, \tag{10}$$

for the steady state population $n_s=n_3$ when both electrostatic and rf perturbations are present. The rate of emission of Balmer α radiation would be

$$S(\text{with rf})=f_s n_s\gamma_s=f_s\gamma_s r_s/(\gamma_s+W_{\rm es}+W_{\rm rf}). \tag{11}$$

Similarly, with only the electrostatic perturbation acting we should have

$$S(\text{no rf})=f_s\gamma_s r_s/(\gamma_s+W_{\rm es}). \tag{12}$$

The difference is

$$\begin{aligned}\Delta S&=S(\text{no rf})-S(\text{with rf})\\&=f_s\gamma_s r_s W_{\rm rf}/[(\gamma_s+W_{\rm es})(\gamma_s+W_{\rm es}+W_{\rm rf})].\end{aligned} \tag{13}$$

If $W_{\rm es}(=W_{23})$ were zero this would be equivalent to the expression given in Part I, Eq. (4) evaluated on the above assumption of negligible $3p$ contribution.

The solution of the full problem can easily be obtained, for instance, from the circuit analog given in Appendix II. In fact, Eq. (13) is already adequate for our purposes, but a still more accurate expression is

$$\Delta S=x(\Delta S)_\infty/[(1+y)(1+y+x)], \tag{14}$$

where the parameters

$$x=W_{13}/\Gamma_1 \tag{15x}$$

and

$$y=W_{23}/\Gamma_1 \tag{15y}$$

measure the transition rates due to rf and Stark perturbations, respectively. The constant

$$(\Delta S)_\infty=(f_s-f_p)\Gamma_1[(r_s/\gamma_s)-(r_p/\gamma_p)] \tag{16}$$

is the signal at full rf saturation when electrostatic perturbations are negligible.

11. Experimental Observations of Electrostatic Quenching

The theory relating to electrostatic quenching which was developed in the previous section can be tested experimentally. Conversely, once its applicability is established the theory can provide a method for measuring the electrostatic fields which exist within the bombardment region—and possibly in other gaseous discharges. The role of such measurements is analogous to that of lifetime measurements in nuclear or paramagnetic resonance experiments where one hopes to learn something about the atomic environment by studying relaxation phenomena.

[3] W. E. Lamb, Jr., Phys. Rev. **85**, 259 (1952), Secs. 68–72.
[4] W. E. Lamb, Jr., and R. C. Retherford, Phys. Rev. **81**, 222 (1951), Sec. 47.

We now develop a convenient graphical method for determination of the quenching parameter y. According to Eq. (14) of Sec. 10 the quantity $x/\Delta S$ should be a linear function of the rf saturation parameter x:

$$x/\Delta S=(1+y)(1+y+x)/(\Delta S)_\infty. \tag{17}$$

Relative measurements of $\mathcal{E}_{\rm rf}^2$ near the interaction region of the bombarder tube determine x to within a constant factor. We write $x=i/i_0$ where i is the measured output of the square law detector probe and i_0 is a constant depending on the frequency and transition being studied. It is found experimentally that $i/\Delta S$ does indeed depend linearly upon i. We write the equation of this line as

$$i/\Delta S=mi+a. \tag{18}$$

According to the theory of Sec. 10 the values of slope and intercept taken from such a plot determine the quantities

$$\text{Slope}=m=(1+y)/(\Delta S)_\infty,$$
$$\text{Intercept}=a=i_0(1+y)^2/(\Delta S)_\infty. \tag{19}$$

If one now plots similar data for a different transition involving the same fine-structure levels but different magnetic sublevels without otherwise altering the rf frequency or instrument gain, the parameters

$$m'=(1+y')/(\Delta S')_\infty, \tag{20}$$

and

$$a'=i_0'(1+y')^2/(\Delta S')_\infty, \tag{21}$$

can be determined. On the very plausible assumption that all magnetic sublevels of a given fine structure level are excited by electron bombardment at the same rate we expect that $(\Delta S)_\infty=(\Delta S')_\infty$, from which it follows that

$$m'=[(1+y')/(1+y)]m. \tag{22}$$

The ratio of the squared matrix elements for the two transitions is known from theory, so that we have

$$i_0'=(|M|^2/|M'|^2)i_0. \tag{23}$$

Hence a' should be given by

$$a'=(|M|^2/|M'|^2)[(1+y')/(1+y)]^2a$$
$$=(|M|^2/|M'|^2)(m'/m)^2a. \tag{24}$$

By comparing this with the observed value of a' we get a test of our quenching theory.

Measurements of this kind are shown in Fig. 12. Data from the $a\alpha$ and $b\beta$ transitions have been plotted as described above. For convenience the horizontal and vertical scales have been altered by constant factors, but this is unimportant, since only ratios are involved. The slope m' of a straight line fitted to the $b\beta$ points is determined, and then the line

$$i/\Delta S=(|M|^2/|M'|^2)(m/m')^2a+m'i \tag{25}$$

is drawn in. The fit is quite satisfactory. From the ratio m'/m, we find $(1+y')/(1+y)=1.42$. If no differential quenching were present, the $b\beta$ points should have fallen along the dotted line.

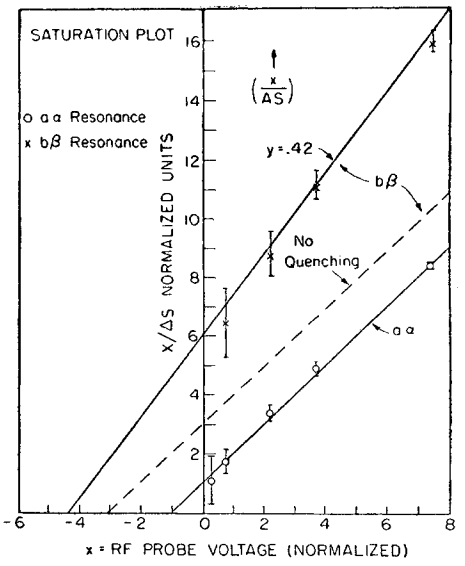

FIG. 12. Rf saturation plot for $a\alpha$ and $b\beta$ resonances. Measurements were made at 3700 Mc/sec, beam current 100 μa, accelerator potential 47 volts. In the absence of electrostatic field the $b\beta$ points would fall along the dashed line.

These measurements can determine only the ratio $(1+y')/(1+y)$. To deduce the quenching parameter y' for the $b\beta$ resonance an assumption regarding y for $a\alpha$ must be made. We tentatively assume that the $a\alpha$ resonance is less strongly quenched than $b\beta$, i.e., $y'\gg y$. This is plausible because the α state energy does not lie close to any p state to which it could be coupled by an electrostatic field. With this assumption, the value $y'=0.42$ is found in the above example. If y were comparable to y' the electrostatic quenching of the β state would be underestimated.

The above measurements of the $b\beta$ resonance maximum were made in a magnetic field of 320 gauss. At this field the βe and βf splittings are, respectively, 284 and 32.6 Mc/sec. The unit fields $\mathcal{E}_{\beta e}$ and $\mathcal{E}_{\beta f}$ are both 0.5 volts/cm, so that according to Eqs. (3) and (15y)

$$y=(\mathcal{E}_\perp/0.5)^2\mathfrak{L}[284/15.3],$$

or

$$y=(\mathcal{E}_{||}/0.5)^2\mathfrak{L}[32.6/15.3], \tag{26}$$

for electric fields assumed perpendicular or parallel to the magnetic field, respectively. For $y=0.42$, we find that the observed quenching could be produced by either a longitudinal field of 0.8 volts/cm, a transverse field of 6.0 volts/cm, or a suitable combination of longitudinal and transverse fields. These measurements were made under conditions which were regarded as "bad" and in view of the large Stark shifts then seen in resonance peaks the value of 6.0 volts/cm is not unreasonable.

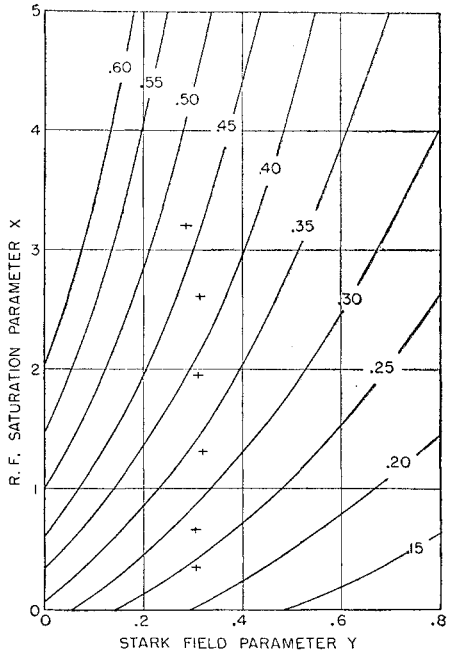

FIG. 13. Curves $R(x,y)=$Constant. After the ratio R and the rf parameter x are experimentally determined the quenching parameter y may be read from the plot. The experimental points were obtained from resonances at 3400 Mc/sec, beam current 50 μa, accelerator potential 44 volts, pressure about 7 microns.

Determination of the quenching parameter y may be simplified as follows. According to the foregoing theory, y is uniquely determined by the ratio of the signal strengths of $b\beta$ and $a\alpha$, provided that the rf saturation parameter x for transition $a\alpha$ is known and assuming the $a\alpha$ resonance is not quenched. We write

$$R(x,y)=(\Delta S)_{b\beta}/(\Delta S)_{a\alpha}$$
$$=\tfrac{1}{3}(1+x)/[(1+y)(1+y+\tfrac{1}{3}x)]. \quad (27)$$

A family of $R=$constant curves is shown in Fig. 13. For low rf amplitude and no quenching, $R=\frac{1}{3}$. When $x=1$ ($a\alpha$ resonance 50% saturated), $R=0.50$ in the absence of quenching. Experimental points, taken on one afternoon, shown in Fig. 12, confirm the fact that the quenching parameter y is not appreciably changed by an increase of rf power up to 75% of complete saturation. These points were obtained under "good" conditions at a rather high pressure (27×10^{-3} mm Hg). They correspond to a transverse electric field of 0.8 volts/cm. This value is lower by a factor of four than that needed to explain our average, or typical Stark shift under similar conditions (See Sec. 18). A possible explanation is that at this high pressure the α state is quenched by ions, increasing the ratio R and thus lowering our estimate for the electric field. (See Appendix III.)

In a further attempt to establish the validity of our interpretation of intensity ratios in terms of electrostatic fields, the following measurements were performed: a frequency was chosen such that the $b\beta$ resonance occurred near 171 gauss, i.e., near the field where the β and e levels cross. With bombardment conditions held constant, the ratio R was measured, and the rf saturation parameter x deduced from the degree of power broadening of $a\alpha$. Using these data, we could calculate y from Eq. (27). The measurements were then repeated at other frequencies such that the βe splitting varied from 0 to 40 Mc/sec. According to Eq. (26), y should exhibit a Lorentzian dependence on the βe splitting. The results of such a test are shown in Fig. 14(a), where the experimental points are fitted with a single arbitrary parameter: the transverse component of electric field equal to 0.48 volt/cm. As before, this field is lower than that required to explain the shifts in our best line center data, and again it may be that the α state is partially quenched by ions.

A similar set of measurements were made near the βf crossing point (357 gauss). In this region $b\beta$ should be sensitive to the longitudinal component of electric field. The results, shown in Fig. 14(b), seem to bear no relation to our quenching theory. If we were to interpret these data to mean that a negligible longitudinal field is present, then the transverse component required to account for the appreciable observed quenching so far from the βe crossing is about 6 volts/cm. Such a large field would be compatible with that found from the data analyzed in Fig. (12).

Our measurements relating to quenching are for the most part internally consistent but they yield electric fields which vary from one run to the next in ways which are not readily correlated with the state of the apparatus, and were usually too low to account for the "Stark" shift in our best data. Further measurements along these lines, in which all physical parameters of the bombarder are rigidly controlled and systematically

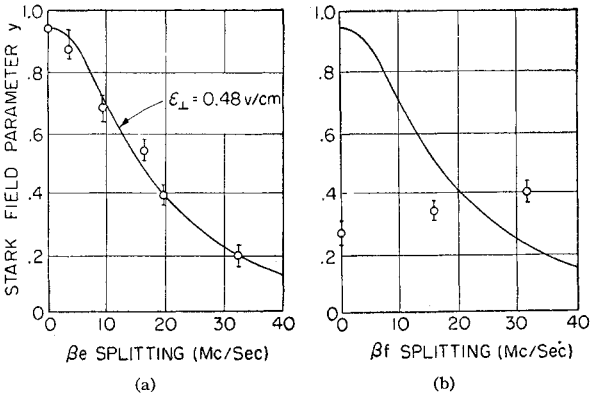

FIG. 14. (a) Quenching parameter y vs βe level separation. The solid curve is a Lorentzian function with width at half height 17 Mc/sec. Experimental conditions were frequency 3300–3340 Mc/sec, beam current 17 μa; accelerator potential 50 volts. (b) Quenching parameter vs βf level separation. The solid curve is the same as that of Fig. 14 (a) and is shown only for comparison. The data would be compatible with the presence of a transverse electric field of about 6 volt/cm and a negligible longitudinal electric field.

varied would be desirable in future work designed specifically to study quenching effects.

E. PANORAMIC LINE TRACES

13. $n=3$ Resonances

(a) $3d-3p$ resonances

A typical recorder trace showing the group of low-frequency resonances (535 Mc/sec) is presented in Fig. 15. Matrix elements for βe and αf are identical, and these resonances are each about 50% saturated. The "chasm" to the left of αf is the cyclotron resonance which made accurate measurement of the line center of αf difficult. The hump to the left of H_c is caused by the π-type transition αe. The circled portion is shown enlarged after subtracting the wing of the βe resonance. From saturation measurements, the rf amplitude is known, and one may calculate the intensity of the $3d-3p$ resonances relative to αf on the assumption that all fine structure sublevels are excited at the same rate. These values for the $3d-3p$ resonances (multiplied by a common factor of 1.1 to improve the fit) were used in drawing the smooth curves of the insert. In view of the difficulties with noise and overlapping resonances, the fit is taken as support for the hypothesis that the $3s$ and $3d$ levels are excited at equal or at least comparable rates.

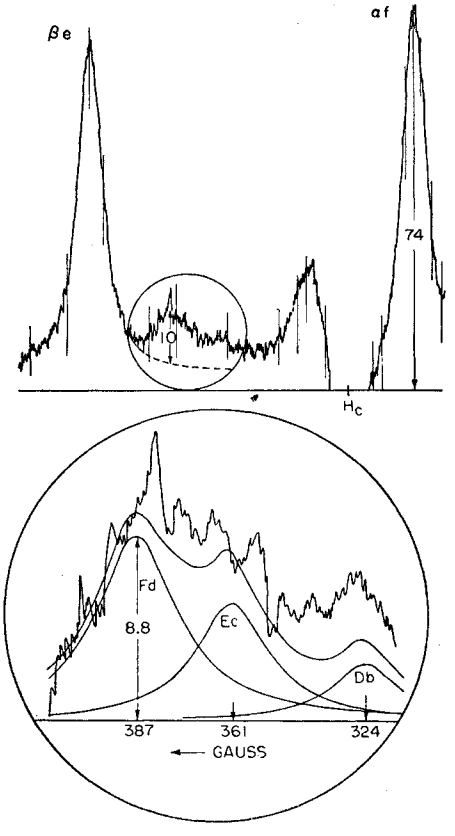

FIG. 15. Low-frequency resonances. The αf and βe resonances are known to be 50% saturated. Strengths of the $3P-3D$ resonances are nearly those expected if the $3S$ and $3D$ sublevels are excited at equal rates. The rf frequency was 535 Mc/sec.

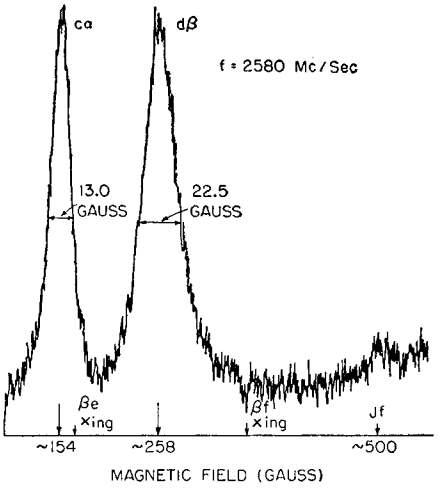

FIG. 16. Recorder trace at 2580 Mc/sec. The $d\beta$ resonance is strongly quenched. Transverse or longitudinal fields of 6.6 or 3.3 volts/cm, respectively, would account for the observed quenching.

(b) *Resonances at 2580 Mc/sec*

Another pair of resonances $d\beta$ and $c\alpha$, which could be used like the $a\alpha$ and $b\beta$ transitions for quenching studies, are shown in Fig. 16. In this case, the squared element for $d\beta$ is larger than that for $c\alpha$ by a factor of 3. The $c\alpha$ resonance is known to be 67% saturated, from which one finds that $d\beta$ should be 86% saturated, or 1.3 times stronger. Using the analysis of Sec. 11 one might conclude that a transverse electrostatic field near 5 volts/cm could be responsible for weakening the $d\beta$ resonance.

14. $n=4$ Resonances

When the H_α interference filter was replaced by one with a transmission band centered on the second Balmer line $H_\beta(\lambda=4861$ A) our apparatus became suitable for observation of $n=4$ fine-structure resonances. A trace showing several such resonances at a frequency of 525 Mc/sec is displayed in Fig. 17.

The $n=4$ resonances were extremely weak. At full saturation the largest resonances shown corresponded to a change of only 0.1% in the H_β intensity. This is to be compared with the theoretical value of 4.7% based upon lifetimes for the unmixed $n=4$ states. Despite various uncertainties, such as background molecular light which could pass the interference filter, one is tempted to conclude that the $n=4$ population differences are weakened by electrostatic fields, ionic effects or some combination of both. This conjecture is further strengthened by the fact that a second attempt to observe the $n=4$ resonances made several days later at a higher beam current was unsuccessful. It is con-

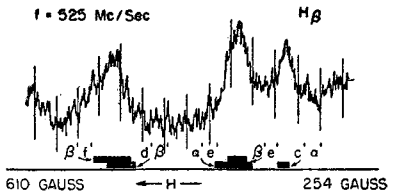

FIG. 17. $n=4$ fine-structure resonances. These were weaker than $n=3$ resonances by more than a factor of ten. Both $P_{\frac{1}{2}}-S_{\frac{1}{2}}$ and $P_{\frac{3}{2}}-S_{\frac{1}{2}}$ resonances are present in the trace. The heavy lines at bottom locate the resonances according to the theoretical for mula assuming an electromagnetic level shift $4\,^2P_{\frac{1}{2}}-4\,^2S_{\frac{1}{2}}$ of 133 Mc/sec.

sistent with the estimates of ion quenching given in Appendix III that the $n=4$ states should be strongly quenched in our apparatus.

The $n=4$ fine structure is smaller than the $n=3$ in the ratio $3^3/4^3=27/64$. Let $E(n=3, H)$ be the Zeeman energy dispalcement of some $n=3$ state. Then in good approximation the Zeeman energy of the corresponding $n=4$ state is given by

$$E(n=4, H)=(27/64)E(n=3, 64H/27). \quad (28)$$

The success with which the $n=4$ resonances were located and identified from this theoretical formula supports the conclusion that the $4\,^2P_{\frac{1}{2}}-4\,^2S_{\frac{1}{2}}$ level splitting ($\approx$133 Mc/sec) does not differ from the theoretical value by more than the natural line width ($\approx$13.5 Mc/sec). Measurements of higher precision must await the finding of better ways to control the electric fields within the apparatus.

F. LINE CENTER DETERMINATIONS

15. Program of Measurements

The following routine for line center measurements was adopted. Two working points, H_1 and H_2, near the points of inflection of the Lorentzian curve, were selected so that the signal strengths agreed to within 2%. A tentative value for the line center was then $\frac{1}{2}(H_1+H_2)$. The signals at H_1 and H_2 were then determined accurately by alternate measurements at the two points. Usually six to eight alternations of 6 minutes each were made. The slope at the working points was then determined from a panoramic recorder trace, and the tentative line center value was shifted by a small amount corresponding to the slightly different signals at the two working points.

Observation of the $a\alpha$ resonance yielded our most precise result. For this the frequency was chosen so that the $b\beta$ resonance occurred near the βe crossing point. The $b\beta$ resonance was then partially quenched so that overlap of $b\beta$ onto $a\alpha$ was minimized. From the relative intensity of $b\beta$ a sensitive indication of the transverse component of the electric field was provided. The other transition chosen for precision studies was βe at magnetic fields well above the βe crossing field.

In most runs the rf power was chosen to produce 50% saturation ($x=1$) of the resonance. At this power level the line is broadened by a factor $\sqrt{2}$. Arguments based upon the line shape formula lead one to conclude that optimum signal-to-noise ratio for measurements of a line center is obtained at the 67% saturation level ($x=2$). However, this neglects possible overlap from weak resonances and the increases possibility of introducing error caused by some poorly understood field dependent variation. As a compromise the 50% saturation level was adopted for most measurements, although it was varied on occasion, a test for unsuspected sources of error.

16. Sources of Error and Corrections

Consideration was given to the following possible sources of error: (1) Stark effect (see Sec. 10); (2) overlap with neighboring resonances; (3) quenching asymmetry (variation of y across resonance); (4) variation of the rf matrix elements;[5] (5) Paschen-Back curvature; (6) electron plasma rf shielding effect; (7) magnetic dependence of the electron optics; (8) cyclotron resonance; (9) Bloch-Siegert shift;[6] and (10) hyperfine structure in deuterium.

All but the first five effects were found incapable of producing a shift larger than 0.02 Mc/sec in our final result. With conditions carefully chosen, effects (2) and (3) were made small (<0.1 Mc/sec). The fourth and fifth do not contribute anything for the $a\alpha$ resonance. Stark shift (1) was thus the dominant correction (and source of error) in our result.

17. Line Center Data

Results from the runs of *a priori* high quality are shown in Table III. Data in which abnormally large Stark fields manifested themselves either by strong quenching of the $b\beta$ resonance or by large shifts dependent on beam energy have been rejected. The variance ΔS attributable to noise is associated with each result, and averages are formed with weighting factors $(\Delta S)^{-2}$.

G. RESULTS AND DISCUSSION

18. Correction for Stark Shift

The disagreement of 1.32 Mc/sec between level shift values as deduced from the $a\alpha$ and βe transitions is attributed primarily to Stark effect. For an electric field $\mathcal{E}_\perp$ perpendicular to the static magnetic field, a negative correction of $0.028\mathcal{E}_\perp^2$ Mc/sec is to be applied to the $a\alpha$ result and a positive correction of $0.10\mathcal{E}_\perp^2$ Mc/sec to the βe result. On supposing that the dominant electric field is transverse, electrostatic in origin and the same for all runs, a field of 3.2 volt/cm would shift the results for the $a\alpha$ and βe runs into agreement at

[5] Reference 3, Sec. 63.
[6] F. Bloch and A. Siegert, Phys. Rev. **57**, 522 (1940).

$\mathcal{S}_D(n=3)=315.21$ Mc/sec. A more plausible assumption is that the electric field is caused primarily by atomic motion across the magnetic field, i.e., $\boldsymbol{\mathcal{E}}_\perp=(\mathbf{v}/c)\times\mathbf{B}$. The two averaged results are then brought into agreement for a root mean square atomic speed corresponding to 0.71 ev for the deuterium atoms. With this assumption, the correction to the $a\alpha$ data is relatively small (−0.11 Mc/sec) (because the magnetic field is smaller than for βe), and the resulting level shift is

$$\mathcal{S}_D(n=3)=315.39 \text{ Mc/sec.}$$

Since the distribution of atomic velocities resulting from the dissociation of the molecule is unknown, and since our quenching measurements failed to establish a unique and reproducible measurement of electric field, detailed Stark-shift correction for each run is impossible. The proper value for the corrected result presumably lies somewhere between 315.21 and 315.39 Mc/sec. Since we are unable to give decisive arguments favoring one value over the other the final value is taken midway between them. Thus we find $\mathcal{S}_D(n=3)=315.30$ Mc/sec. The uncertainty of the Stark-shift correction is reflected in the limit of error assigned to the final result.

19. Limits of Error

The variance for results derived from the $a\alpha$ transition is 0.13 Mc/sec, which is about three times larger than that which would be caused by noise alone. The increased variance is attributed to electric perturbations which vary with experimental conditions in an unknown way. Our confidence limits for the final result are estimated as follows: Maximum probable error due to data statistics (twice mean variance) ±0.25 Mc/sec, frequency measurement ±0.10 Mc/sec, magnetic field measurement ±0.10 Mc/sec, Stark-shift correction ±0.25 Mc/sec, all other sources of asymmetry ±0.10 Mc/sec. The sum of the absolute values is taken as "limit of error," ±0.80 Mc/sec.

TABLE III. Summary of data. In computing the level shift $\mathcal{S}_D$ from the data for the $a\alpha$ transition a theoretical value $\Delta E=3250.70$ Mc/sec for the fine structure interval $3\,^2P_{\frac{3}{2}}-3\,^2P_{\frac{1}{2}}$ has been employed.

Frequency (Mc/sec)	Beam energy volts	Beam current μa	Experimental level shift ($n=3$) Mc/sec
		$a\alpha$ resonance	
3320.00±0.1	45	100	315.50±0.12
3320.00	21	100	315.50±0.16
3360.00	46	50	315.64±0.23
3360.00	46	100	315.28±0.19
3360.00	30	100	315.42±0.23
3360.00	25	100	315.42±0.10
3360.00	23	100	315.28±0.23
3360.00	45	60	315.42±0.13
3360.00	45	100	315.78±0.12
		Weighted average	315.50±0.05
		βe resonance	
650.00±0.1	24	30	314.08±0.13
650.00	23	50	314.43±0.09
650.00	23	100	314.34±0.08
650.00	22	100	314.08±0.15
650.00	45	100	313.38±0.15
650.00	23	170	314.43±0.19
635.00	24	30	314.37±0.15
635.00	24	80	313.89±0.12
		Weighted average	314.18±0.04

TABLE IV. Summary of level shift results and comparison with theoretical values, in Mc/sec.

	Theoretical	Experimental
($n=3$) $3\,^2S_{\frac{1}{2}}-3\,^2P_{\frac{1}{2}}$	315.34	315.30±0.80
($n=3$) $3\,^2P_{\frac{3}{2}}-3\,^2P_{\frac{1}{2}}$	3250.70	3250.7 ±2.0
($n=3$) $3\,^2P_{\frac{1}{2}}-3\,^2D_{\frac{3}{2}}$	5.34	5.0 ±10
($n=4$) $4\,^2S_{\frac{1}{2}}-4\,^2P_{\frac{1}{2}}$	133.163	133.0 ±10

20. Final Results and Discussion

The final corrected value for the $3\,^2S_{\frac{1}{2}}-3\,^2P_{\frac{1}{2}}$ level shift in deuterium is 315.30±0.80 Mc/sec. The 0.80 Mc/sec uncertainty is believed to represent the maximum limit of error. It should be possible to obtain a value with a limit of error of 0.10 Mc/sec by making fairly obvious improvements in our work. For such a program, the apparatus would certainly require modification to improve its pressure stability and range of magnetic field. It would also be necessary to make further studies of shift and quenching effects, together with extensive numerical analysis of results from many different transitions. Possibly, accurate study of $n=4$ fine-structure resonances could provide a more significant measurement of Stark shifts which could in turn be used to correct the $n=3$ data. As we have mentioned, however, the $n=4$ resonances were very weak in our apparatus.

It is also possible to give an experimental value for $\Delta E(3\,^2P_{\frac{3}{2}}-3\,^2P_{\frac{1}{2}})$ based on the foregoing data. If no Stark corrections were needed, one would interpret the difference of 1.32 Mc/sec in the two values of $\mathcal{S}_D$ in Table III as meaning that ΔE had a value 1.32 Mc/sec lower than the theoretical value 3250.70 Mc/sec. From the estimates in Appendix III we regard it as unlikely that the Stark shifts are larger than twice as much as indicated above. If they were so large, the value of ΔE would be 1.32 Mc/sec higher than the theoretical value. With an allowance for other sources of error we set $\Delta E=3250.7\pm2.0$ Mc/sec.

The results of the present work are summarized in Table IV.

ACKNOWLEDGMENTS

This work owes much to Professor T. M. Sanders, Jr., who designed and assembled much of the equipment and obtained the first $n=3$ resonances. The authors also wish to thank Kenneth Kerwin, who helped take some of the data.

APPENDIX I: POPULATION MATRIX FOR N LEVELS

In the previous paper (Part I) a population matrix ρ was introduced for the theory of a system with two excited levels which decay while a perturbing field caused transitions between them. The theory can easily be generalized for N levels subject to certain perturbations. Let the time-dependent Schrödinger equation be

$$i\hbar\dot{a}_j=\sum_{k=1}^{N}\left(H_{jk}-\frac{i}{2}\hbar\gamma_k\delta_{jk}\right)a_k \quad j=1, 2, \cdots N, \quad \text{(I.1)}$$

where the γ_k are phenomenological decay constants. Let $a_j(t,t_0,n)$ be the solution of (I.1) satisfying the initial conditions $a_j(t_0,t_0,n)=\delta_{jn}$, i.e., $a_j(t,t_0,n)$ is the probability amplitude for the state j if the atoms are put[7] into state n at time $t=t_0$. The corresponding population matrix is given by

$$\rho_{jk}(t)=\sum_{n=1}^{N}\int_{-\infty}^{t}dt_0\, r_n(t_0)a_k^*(t,t_0,n)a_j(t,t_0,n), \quad \text{(I.2)}$$

with diagonal elements $\rho_{jj}(t)$ representing the population of atoms in state j at time t after excitation of the various states n at rates $r_n(t_0)$.

Using the definition of ρ together with the wave equation (I.1), a differential equation satisfied by the matrix $\rho(t)$ can be derived. This is most compactly expressed in matrix notation as

$$\dot{\rho}=-(i/\hbar)(H\rho-\rho H)-\tfrac{1}{2}(\Gamma\rho+\rho\Gamma)+r, \quad \text{(I.3)}$$

where Γ and $r(t)$ are diagonal[7] matrices with $\Gamma_{jk}=\gamma_j\delta_{jk}$ and $r_{jk}=r_j\delta_{jk}$, respectively.

Equation (I.3) differs from the analogous expression for the density matrix of Dirac and von Neumann by the addition of the anticommutator $\Gamma\rho+\rho\Gamma$ to allow for damping and the inhomogeneous excitation term r. We shall refer to Eq. (I.3) as the Boltzmann equation because of the analogy to the classical equation for density in phase space.

[7] More generally, one should consider the possibility of off-diagonal excitation, i.e., that at t_0 the atom is excited by a pulse to a state which is a linear combination of the states which we used. Thus, in optical pumping experiments the exciting radiation may have a polarization inclined to the axis of quantization and the various magnetic sublevels may be excited in a coherent fashion. In the case of atomic hydrogen, excitation of $3s$ and $3p$ by an electron of energy near threshold would be coherent. This would lead to equations of the form considered above, but with the matrix r nondiagonal. The off-diagonal elements of r may not average to zero when one takes all excitation processes into account. With the employed method of production of excited atoms by bombardment of molecules there are additional possibilities for averaging out of the off-diagonal elements of r. Even if these did not vanish, it is unlikely that they would contribute a noticeable effect in the measurements made in this paper, although their presence might cause observable light beats. Breit [G. Breit, Revs. Modern Phys. **5**, 91 (1933); see also G. Breit and I. S. Lowen, Phys. Rev. **46**, 590 (1934)] has shown that the damping matrix Γ is diagonal in the representation which we have used in this paper.

The rate of emission of photons of the sort detected may be taken to be[8]

$$S=\sum_{j=1}^{N}f_j\gamma_j\rho_{jj}, \quad \text{(I.4)}$$

where the f_j are appropriate branching ratios.

It was shown in Part I, Sec. 2, how Eq. (I.3) could be solved in case two levels[9] were coupled by a rotating wave perturbation. This led to a restatement of the full quantum mechanical problem in terms of two coupled "rate" equations involving only diagonal elements of the ρ matrix.

In a treatment of the three-level problem for this paper, we again found the notation of rate constants to be very helpful, and were led to ask more generally: when is the notion of "transition rates" applicable? Within the framework of the model provided by Eq. (I.3), the simplest answer is: if the Hamiltonian is independent of time then the notion of transition rates can be rigorously applied. Fortunately this severe condition on the Hamiltonian may be somewhat weakened. In certain cases a time dependence may be eliminated from the effective Hamiltonian by a canonical transformation.

Let $U(t)$ be a time-dependent unitary transformation having diagonal form. The transformed ρ matrix defined by

$$\sigma=U^\dagger\rho U, \quad \text{(I.5)}$$

obeys a differential equation

$$\dot{\sigma}=-\{(\tfrac{1}{2}\Gamma\pm iU^\dagger HU-\dot{U}^\dagger U)\sigma+\sigma(\tfrac{1}{2}\Gamma-iU^\dagger HU-U^\dagger\dot{U})\}+r. \quad \text{(I.6)}$$

Since Γ and r are diagonal they are unaffected by the diagonal canonical transformation. The explicit time dependence will disappear from Eq. (I.6) provided a U matrix can be found such that

$$\Omega=\tfrac{1}{2}\Gamma+iU^\dagger HU-\dot{U}^\dagger U \quad \text{(I.7)}$$

is a matrix independent of time. We consider only cases where the required U exists, and take Eq. (I.6) in the form

$$\dot{\sigma}=-(\Omega\sigma+\sigma\Omega^\dagger)+r, \quad \text{(I.8)}$$

where Ω and its Hermitian adjoint $\Omega^\dagger$ are independent of time.

[8] More generally for applications of the density matrix method to other problems, the observed signal could be written in the form $S=\text{Trace}\,(Q\rho)$ where Q is a suitable matrix.

[9] Our two-level problem can be put in one-to-one correspondence with that of a magnetization vector $\mathbf{M}$ described by Bloch's phenomenological equations of nuclear induction. One sets $\rho=\frac{1}{2}(M_0I+\mathbf{M}\cdot\boldsymbol{\sigma})$, where I, σ_x, σ_y, and σ_z are the usual 2×2 matrices. In a quasi-steady state, with rotating wave perturbation, M_0 becomes $(r_1/\gamma_1+r_2/\gamma_2)$ and is the analog of the magnetization in thermal equilibrium. Bloch's longitudinal and transverse relaxation times have counterparts

$$T_1=\tfrac{1}{2}(1/\gamma_1+1/\gamma_2) \quad \text{and} \quad T_2=2/(\gamma_1+\gamma_2),$$

with $T_1\geqslant T_2$ and equality only if $\gamma_1=\gamma_2$.

In a steady state we have

$$\Omega\sigma+\sigma\Omega^\dagger=r, \tag{I.9}$$

an equation which has been treated in the mathematical literature.[10] Since the decay constants γ_j are all positive a unique solution exists and is given by

$$\sigma=\int_0^\infty \exp(-\Omega s)r\exp(-\Omega^\dagger s)ds. \tag{I.10}$$

As one might suppose, the steady state populations $\sigma_{jj}\equiv\sigma_j$ are linear combinations of the production rates

$$\sigma_j=\sum_{k=1}^N K_{jk}r_k, \tag{I.11}$$

where

$$K_{jk}=\int_0^\infty [\exp(-\Omega s)]_{jk}[\exp(-\Omega^\dagger s)]_{kj}ds$$

$$=\int_0^\infty |[\exp(-\Omega s)]_{jk}|^2 ds. \tag{I.12}$$

The coefficients K_{jk} are positive and belong to a real symmetric matrix K. An additional important property of the K matrix is obtained in the following manner. For the case of equipartition (i.e., σ=unit matrix), Eq. (I.9) gives

$$\Omega+\Omega^\dagger=r, \tag{I.13}$$

so that when $\sigma=I$ we have $r=\Gamma$. This means that if each level is excited at a rate proportional to its respective decay constant all populations are equal for any Hamiltonian leading to a time independent Ω. Upon insertion of $\sigma_j=1$ and $r_k=\gamma_k$ in Eq. (I.11) one finds

$$\sum_{k=1}^N K_{jk}\gamma_k=1, \tag{I.14}$$

i.e., the product $K\Gamma$ is a positive stochastic matrix.

We now enquire whether constants W_{jk}, $j\neq k$ can be found such that the $\dot\sigma_j$ satisfy a set of rate equations of the form

$$0=-\gamma_j\sigma_j+\sum_{k\neq j} W_{jk}\sigma_k-\sigma_j\sum_{k\neq j} W_{kj}+r_j. \tag{I.15}$$

To facilitate the discussion we introduce a matrix W whose off diagonal elements are the W_{jk} of Eq. (I.15) and whose diagonal elements W_{jj} are defined by the equations

$$W_{jj}+\sum_{k\neq j} W_{kj}=\sum_{k=1}^N W_{kj}=0. \tag{I.16}$$

We now introduce column vectors $\boldsymbol{\sigma}$, $\mathbf{r}$, $\boldsymbol{\gamma}$ with components σ_j, r_j, γ_j, respectively, and also $\mathbf{d}$ with $d_j=1$.

[10] M. Rosenblum, Duke Math. J. **23**, 263 (1956).

In matrix algebra notation we then have

$$\boldsymbol{\sigma}=K\mathbf{r}, \tag{I.17a}$$

$$K\boldsymbol{\gamma}=\mathbf{d}, \tag{I.17b}$$

$$\Gamma\mathbf{d}=\boldsymbol{\gamma}, \tag{I.17c}$$

and are asking whether a matrix W exists such that

$$(W-\Gamma)\boldsymbol{\sigma}+\mathbf{r}=0, \tag{I.18}$$

with

$$\tilde W\mathbf{d}=0. \tag{I.19}$$

If so, we can substitute (I.17a) into (I.18) and find

$$[(W-\Gamma)K+I]\mathbf{r}=0. \tag{I.20}$$

Since the components of $\mathbf{r}$, although positive, are otherwise arbitrary, the matrix equation

$$(W-\Gamma)K+I=0, \tag{I.21}$$

must hold. Hence if W exists it is given by

$$W=\Gamma-K^{-1} \tag{I.22}$$

and can be calculated from the K matrix of Eq. (I.12). In fact we see that if K^{-1} exists, a matrix W can be obtained from (I.22) which will reduce (I.20) to an identity. The symmetry of W follows from that of K. The other condition (I.19) on W, i.e., $(\Gamma-K^{-1})\mathbf{d}=0$ or $K^{-1}\mathbf{d}=\boldsymbol{\gamma}$ is also satisfied by virtue of (I.17).

It remains to discuss whether the matrix K has an inverse. If Ω is a diagonal matrix, the K given by (I.12) is diagonal and certainly has an inverse. For Ω sufficiently different from a diagonal matrix, it might happen that det $K=0$ so that K^{-1} would not exist. However, a slight change in Ω would, in general, again lead to a nonsingular K matrix. Hence we may say that rate constants will exist for "almost all" problems with time independent Ω's.

APPENDIX II: THREE-LEVEL PROBLEM

The needs of the present paper will be served if we consider in more detail only a three level problem as shown in Fig. 10. An rf perturbation $2R\cos\nu t$ causes transitions between states 1 and 3, and a static electric field couples states 2 and 3 with a matrix element V. The states have decay constants γ_j and separations denoted by ω_{jk}.

If we consider only the rotating wave part of $2R\cos\nu t$ which is able to cause resonance, the Hamiltonian matrix becomes

$$H=\begin{pmatrix} \omega_{13} & 0 & \mathrm{Re}^{-i\nu t} \\ 0 & \omega_{23} & V \\ \mathrm{Re}^{i\nu t} & V & 0 \end{pmatrix}. \tag{II.1}$$

We point out in passing that this problem can be transformed by a unitary transformation $U(t)$ into another problem in which the perturbing frequencies are $\nu-\mu/2$ and $-\mu$ instead of ν and 0, with energy levels ω_{12}, $\omega_{23}-\mu/2$ and μ instead of ω_{12}, ω_{23}, and 0. The

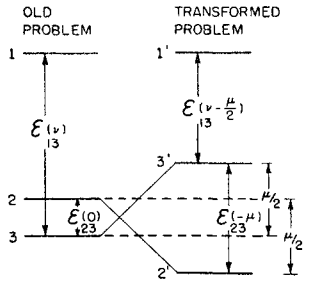

FIG. 18. Class of problems related by a trivial transformation. When antiresonant terms are neglected, then results derived for our problem are directly applicable to a class of problems in which common level is connected to two others by perturbations with arbitrary frequencies.

appropriate transformation matrix $U(t)$ is diagonal, with elements 1, $\exp(-\frac{1}{2}i\mu t)$, and $\exp(+\frac{1}{2}i\mu t)$. The Γ and r terms of the Boltzmann equation (I.3), being diagonal matrices, are unaltered by the diagonal transformation $U(t)$. The relation between this new problem and the problem as originally phrased is shown in Fig. 18. As a special case, one might set $\mu=\frac{2}{3}\nu$. The new problem now relates to a physical system having three energy levels $1'$, $2'$, and $3'$ which are perturbed by a single frequency $(2/3)\nu$. When the levels 2 and 3 (old problem) are nearly degenerate, the level $3'$ lies about midway between $1'$ and $2'$. Under these conditions, "double-quantum" transitions $1\leftrightarrow 2$ can occur when $\nu\sim\omega_{13}$, and such phenomena have been observed in magnetic resonance experiments.[11] As an example of the "old" problem we mention the sharp "forbidden" resonances between the long-lived $2s$ states which were observed by Lamb and Retherford.[3,4]

In the problem, as originally stated, it is readily verified that the diagonal transformation

$$U(t)=[e^{-i\nu t},1,1]$$

applied to (I.6) eliminates the time-dependent terms completely and the effective Hamiltonian $U^\dagger HU+i\dot{U}^\dagger U$ for use in Eq. (I.3) becomes

$$H=\begin{bmatrix}\omega_{13}-\nu & 0 & R\\ 0 & \omega_{23} & V\\ R & V & 0\end{bmatrix}. \tag{II.2}$$

This is a Hamiltonian of the type for which the general theory developed in Appendix I applies and hence a set of rate equations with symmetrical coefficients W_{jk} should exist. A first approximation to the W_{jk} may easily be obtained from a perturbation expansion of Eq. (I.12). However, we require terms beyond the first for analysis of the measurments. In problems involving only three levels it appears simpler to solve Eqs. (I.3) in closed form by straightforward algebraic manipulations.

[11] P. Kusch and V. W. Hughes, *Encyclopedia of Physics* (Springer-Verlag, Berlin, 1959), Vol. 3711, p. 67.

(a) *Evaluation of Rate Constants*

The elements of Eqs. (I.3) written out in detail are

$$\begin{aligned}
\dot\rho_{11}&=-\gamma_1\rho_{11}-2R\,\mathrm{Im}\rho_{13}+r_1,\\
\dot\rho_{22}&=-\gamma_2\rho_{22}+2V\,\mathrm{Im}\rho_{23}{}^*+r_2,\\
\dot\rho_{33}&=-\gamma_3\rho_{33}+2R\,\mathrm{Im}\rho_{13}-2V\,\mathrm{Im}\rho_{23}{}^*+r_3,\\
\dot\rho_{12}&=(\Delta_{12}-\nu)\rho_{12}-V\rho_{13}+R\rho_{23}{}^*,\\
\dot\rho_{13}&=-V\rho_{12}+(\Delta_{13}-\nu)\rho_{13}-R(\rho_{11}-\rho_{33}),\\
\dot\rho_{23}&=-R\rho_{12}+\Delta_{23}{}^*\rho_{23}{}^*+V(\rho_{33}-\rho_{22}),
\end{aligned} \tag{II.3}$$

where

$$\Delta_{jk}=\omega_{jk}-i\gamma_{jk}, \tag{II.4a}$$

and

$$\gamma_{jk}=\tfrac{1}{2}(\gamma_j+\gamma_k). \tag{II.4b}$$

Assuming that the off-diagonal elements of $\dot\rho$ may be neglected, the last three of Eqs. (II.3) may be written in vector form

$$B\mathfrak{y}=A\mathfrak{o}, \tag{II.5}$$

where the vectors $\mathfrak{o}$ and $\mathfrak{y}$ have components ρ_{11}, ρ_{22}, ρ_{33}, and ρ_{12}, ρ_{13}, $\rho_{23}{}^*$ respectively, and the matrices B and A are given by

$$B=\begin{bmatrix}\Delta_{12}-\nu & -V & R\\ -V & \Delta_{13}-\nu & 0\\ R & 0 & -\Delta_{23}{}^*\end{bmatrix}, \tag{II.6}$$

and

$$A=\begin{bmatrix}0 & 0 & 0\\ R & 0 & -R\\ 0 & -V & V\end{bmatrix}, \tag{II.7}$$

respectively. The off-diagonal elements of ρ may then be expressed in terms of the diagonal elements by $\mathfrak{y}=B^{-1}A\mathfrak{o}$ and substituted in the first three of Eqs. (II.3). The result is a vector equation containing only diagonal elements of the density matrix

$$=\dot{\mathfrak{o}}-\Gamma\mathfrak{o}-2\,\mathrm{Im}(\tilde{A}B^{-1}A)\mathfrak{o}+\mathbf{r}. \tag{II.8}$$

Here $\tilde{A}$ denotes the transposed matrix of A.

We define a matrix W by

$$W_{jk}=-2\,\mathrm{Im}(\tilde{A}B^{-1}A)_{jk}, \tag{II.9}$$

whose symmetry follows from that of B. Since the sum of elements in any row of A is zero, the same is true of W, i.e.,

$$\sum_{k=1}^{N}W_{jk}=0, \tag{II.10}$$

or

$$W_{jj}=-\sum_{k\neq j}W_{jk}. \tag{II.11}$$

Using these properties of the W matrix, Eq. (II.8) may be cast in the form of the rate equation

$$\dot\rho_{jj}=-\gamma_j\rho_{jj}+\sum_{k\neq j}W_{jk}\rho_{kk}-\rho_{jj}\sum_{k\neq j}W_{jk}+r_j. \tag{II.12}$$

To evaluate the rate constants it is only necessary to perform the operations indicated in the definitions

(II.9). The results are

$$W_{13}=2R^2\,\mathrm{Im}\{[1-V^2(\Delta_{12}-\nu-i\gamma_3)/D]/(\Delta_{13}-\nu)\},$$
$$W_{23}=-2V^2\,\mathrm{Im}\{[1-R^2(\Delta_{12}-\nu-i\gamma_3)/D]/\Delta_{23}^*\},$$
$$W_{12}=2R^2V^2\,\mathrm{Im}\{1/D\}, \qquad \text{(II.13)}$$

where

$$D=\Delta_{23}^*[(\Delta_{12}-\nu)(\Delta_{13}-\nu)-V^2]+R^2(\Delta_{13}-\nu). \qquad \text{(II.14)}$$

Contrary to what might be expected, the W's are not all necessarily positive, although they seem to be positive in most interesting cases.

In the general case the functional form of the above rate constants is very complicated. The character of the resonance effects, implicit in Eqs. (II.13) depends critically on the relative lifetimes of the states involved. We are concerned here primarily with the interaction between $3p$ and $3s$ states of the deuterium atom, which have lifetimes of 5.4 mμ sec and 160 mμ sec, respectively, so that $\gamma_s\sim\gamma_p/30$. In the present applications, states 1 and 2 are p states (b, e or b f) and 3 is the s state β. The regions of Fig. 4 to which the present discussion applied are labelled 1, 2, 3, 5, and 7. For our applications Eqs. (II.13-14) may be simplified by dropping numerically insignificant terms. Thus, with $\gamma_s\ll\gamma_p$ and the rf saturation and Stark quenching parameters x and y no larger than of order unity, we may write

$$D\sim\Delta_{23}^*(\Delta_{12}-\nu)(\Delta_{13}-\nu), \qquad \text{(II.15)}$$

and

$$W_{13}\sim 2R^2\,\mathrm{Im}\{[1-V^2/(\Delta_{13}-\nu)\Delta_{23}^*]/(\Delta_{13}-\nu)\}. \qquad \text{(II.16)}$$

(b) *Stark Effect*

Equation (II.16) may be rearranged to yield

$$W_{13}=2R^2\,\mathrm{Im}\{1/[\Delta_{13}-\nu+(V^2/\Delta_{23}^*)]\}, \qquad \text{(II.17)}$$

correct to first order in V^2. This form implies a shift in the resonance maximum by

$$\delta\omega_{13}=\omega_{23}V^2/(\omega_{23}^2+\gamma_{23}^2), \qquad \text{(II.18)}$$

and an increase in the width parameter from γ_{13} to $\gamma_{13}+\delta\gamma_{13}$ with

$$\delta\gamma_{13}=\gamma_{23}V^2/(\omega_{23}^2+\gamma_{23}^2), \qquad \text{(III.19)}$$

as stated in Sec. 10.

(c) *Solution of Rate Equations. Network Analog*

With the rate constants determined, Eqs. (I.15) should be solved for the steady state populations. The intensity of H_α light and its changes due to square wave modulation of the rf power should then be calculated. The algebraic work is simplified, and more physical insight is provided by working with a network analog of the equations. Constant current sources deliver currents r_j to the three terminals as shown in Fig. 19(a). The steady state populations ρ_j are represented by the voltages of the circled electrodes, with the base line taken at ground potential. The switch is inserted in the branch with W_{13} to allow for the modulation of the rf power.

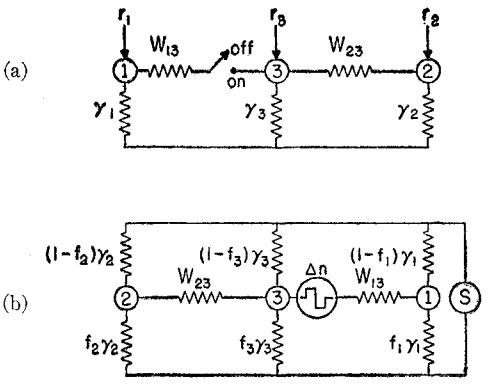

FIG. 19. Network representing the coupled rate equations which result from the quantum mechanical treatment. (a) A small term (large "impedance") connecting terminals 1 and 2 is omitted. The switch represents pulse modulation of the rf power. (b) Further evolution of the network. The square wave current flowing through S is analogous to the observed light modulation in our experiment. It is clear that the excitation rates are relevant only insofar as they determine the "voltage", Δn, across the open switch of Fig. 19(a).

If each of the admittances γ_j is replaced by a parallel combination of admittances $f_j\gamma_j$ and $(1-f_j)\gamma_j$, the intensity of H_α light can be represented by the sum of the three currents flowing through $f_1\gamma_1$, $f_2\gamma_2$, and $f_3\gamma_3$. This can be represented as the current I in Fig. 19(b). Ths signal is then represented by the square wave current which flows through the detector S in Fig. 19(b). Using the compensation theorem,[12] the switch has been replaced by a square wave voltage generator with voltage ΔN equal to the voltage across the switch in Fig. 19(a) when the switch is open. A simple calculation gives for this voltage

$$\Delta N=\rho_3-\rho_1$$
$$=[(\gamma_2+W_{23})r_3+W_{23}r_2]/[\gamma_2\gamma_3+(\gamma_2+\gamma_3)W_{23}]-(r_1/\gamma_1). \qquad \text{(II.20)}$$

The exact solution for this circuit problem is easily obtained, but is unnecessarily complicated. Neglecting some terms of relative order γ_s/γ_p, f_p/f_s, but not necessarily W/γ_s, one gets the result given in Eq. (14) of the text.

APPENDIX III: ESTIMATES OF PERTURBING ELECTRIC EFFECTS

We will give here a number of rough numerical estimates of electrical disturbances acting on the deuterium atoms in our experiment.

(a) *Motional Electrical Field*

It was already mentioned in Part I that a typical value for the velocity of an excited deuterium atom was

[12] *Radiation Laboratory Series* (McGraw-Hill Book Company, New York, 1948), Vol. 8, p. 92.

1×10^6 cm/sec. In moving at right angles through a magnetic field of 100 gauss such an atom would experience an electric field of one volt/cm. Needless to say, the assumed velocity might easily be in error by a factor of two.

(b) *Space Charge Fields in Absence of Neutralization by Positive Ion Formation*

We consider that the electron beam uniformly fills[13] a long circular cylinder with radius $a=\frac{1}{16}$ in. (Fig. 3); the beam is assumed to have an energy of 20 ev and a current of 100 μa. The velocity of such electrons is 2.65×10^8 cm/sec, the number of them per second is 6.25×10^{14} sec^{-1}, corresponding to a flux density 7.9×10^{15} cm^{-2} sec^{-1}. The concentration of primary electrons is 3.0×10^7 cm^{-3}. The resulting space charge electric field is radial, and at the surface of the cylinder it amounts to $\mathcal{E}_1(a)=4.3$ volt/cm. The rms field inside the beam is one half as much. This estimate neglects any depression of the electron beam energy by space charge. On the assumption that the beam is surrounded by a conducting cylinder at cathode potential of radius $b=\frac{5}{8}$ in. the potential at beam center is lower than at the cathode by

$$\delta V=\mathcal{E}_1(a)a[\log_e(b/a)+\tfrac{1}{2}]=1.9 \text{ ev}. \quad \text{(III.1)}$$

The electrons would accordingly have an energy somewhat lower than 20 ev, but not to an extent that would greatly change the estimate of $\mathcal{E}_1(a)$.

The problem is complicated by the presence of secondary electrons, both those emitted from the anode and those generated in the bombardment region. The slowest of the former type will be kept out of the interaction space by space charge repulsion, but faster ones must be taken into account. Hence it is plausible that transverse electric fields somewhat larger than the 4.3 volt/cm estimated above could be produced by electronic space charge. Such fields were invoked at various points in the text to explain the "bad" conditions. If this interpretation is correct, the remedy is to arrange for neutralization of the space charge by positive ion formation. This can be achieved, as noted in the text, by using a higher hydrogen pressure and a higher beam energy for which the cross section for ionization is larger. Further improvement could result from the use of ion trapping electrodes.

(c) *Effects of Positive Ions*

Under suitable conditions one might expect to have neutralization of the electronic space charge by positive ions. Their concentration would then be 3.0×10^7 cm^{-3}. The resulting neutral plasma would still produce local fields which would cause transitions among the fine structure sublevels. Because of their higher velocity, the electrons contribute much less in close encounters with the excited deuterium atoms than do the positive ions. Effects due to electrons will be neglected in the following discussion.

A typical distance between positive ions is 3×10^{-3} cm. At this distance from a stationary positive ion, the electric field is 0.014 volt/cm, and thus effects of static Holtsmark electric fields on the excited deuterium atoms can be neglected. Dynamic effects have been considered for $n=2$ by Purcell[14] and by Seaton.[15] For simplicity, we adapt Purcell's treatment by the method of impact parameters to our problem where $n=3$.

Let the excited atom be initially in sublevel α of the $3\,^2S_{\frac{1}{2}}$ state. It is required to find the probability w' that after an ionic impact of impact parameter b a transition to $3\,^2P_{\frac{1}{2}}$ has occurred. Adapting Purcell's Eq. (6), we write

$$w'=(6)(12)[e^2a_0/(\hbar vb)]^2, \quad \text{(III.2)}$$

where a factor 6 has been inserted since now $n=3$ instead of 2. This expression is valid for $b_s\ll b\ll b_a$ where $b_a=v/\omega'$ is the adiabatic cutoff distance, beyond which the correct expression for w' falls off exponentially. The separation $3\,^2S_{\frac{1}{2}}-3\,^2P_{\frac{1}{2}}$ is denoted by $\hbar\omega'$. Since first order perturbation theory was used in deriving Eq. (III.2) it can be used only for distances $b\gg b_s$ for which the coupling is not too strong. The probability w'' of transitions to $3\,^2P_{\frac{3}{2}}$ is given by an expression like (III.2) with w' replaced by w'' and the factor 12 replaced by 24 since the corresponding squared matrix element is twice that for $3\,^2P_{\frac{1}{2}}$.

The condition for weak coupling may be taken to be $w'+w''\ll1$. In accordance with Purcell's procedure, we take as a generalization valid for $0\lesssim b\ll b_a$ the expressions

$$\begin{aligned} w'&=\tfrac{1}{3}\sin^2(B/b),\\ w''&=\tfrac{2}{3}\sin^2(B/b), \end{aligned} \quad \text{(III.3)}$$

where

$$B^2=(3)(6)(12)(e^2/\hbar c)^2(c/v)^2a_0^2. \quad \text{(III.4)}$$

These reduce to the weak coupling forms when $b\gg B$, and have the requisite property $w'+w''\lesssim1$ in the strong coupling region. The indicated form of oscillatory behavior of w' and w'' is unlikely to be correct in detail, even though w''/w' has the value 2 suggested by the ratio of statistical weights of $3\,^2P_{\frac{3}{2}}$ and $3\,^2P_{\frac{1}{2}}$. However, the region $b\ll B$ does not contribute much to the final estimates.

In order to simplify the calculations we shall ignore the Zeeman splitting of the fine structure and merely use average energy separations between the α state and the $3\,^2P_{\frac{1}{2}}$ and $3\,^2P_{\frac{3}{2}}$ sublevels. For a field of 200 gauss, we take $\omega'/2\pi=500$ Mc/sec and $\omega''/2\pi=2800$ Mc/sec. In order to calculate the adiabatic cutoff distances v/ω, we need the relative velocity of the ions with respect to the excited atoms. The ions are predominantly D_2^+ with approximately thermal velocities, say 10^5

[13] If the cathode area emits electrons nonuniformly the electric fields estimated may be somewhat too low.

[14] E. M. Purcell, Astrophys. J. **116**, 457 (1952).

[15] M. J. Seaton, Proc. Phys. Soc. (London) **A68**, 457 (1954).

cm/sec, while the excited D atoms, as in earlier calculations, have a speed of about 1×10^6 cm/sec. For simplicity we take v to have the latter value. Then $v/\omega'=3\times10^{-4}$ cm and $v/\omega''=5.7\times10^{-5}$ cm.

The cross section for the transition from α to sublevels of $3\,^2P_{\frac{1}{2}}$ is taken as

$$\sigma'=2\pi\int_0^{v/\omega'} w'(b)bdb, \qquad \text{(III.5)}$$

with σ'' given by a similar equation. The neglect of contributions beyond the adiabatic cutoff distances does not cause much error. To a sufficiently good approximation, one finds

$$\sigma'=(2\pi/3)B^2(\tfrac{3}{2}-0.577-\log_e B\omega'/v), \qquad \text{(III.6)}$$

with a similar expression for σ''.

The transition rate when the excited atom moves with speed v through a plasma with ion concentration N_i is

$$W_i=N_i(\sigma'+\sigma'')v. \qquad \text{(III.7)}$$

For the above-mentioned numerical values, $\sigma'=1.9\times10^{-9}$ cm^2, $\sigma''=1.8\times10^{-9}$ cm^2 and $W_i=1.1\times10^5$ sec^{-1}. This rate, which was calculated for an ion concentration $N_i=3\times10^7$ cm^{-3}, is rather small compared to the radiative decay rate of $3\,^2S_{\frac{1}{2}}$ which is $\gamma_s=6.3\times10^6$ sec^{-1}. One would expect that the main consequences of these ionic interactions would be allowed for by a change in the effective γ_s and that Stark shifts would be given approximately by the static Holtsmark contribution already mentioned.

The ion concentration assumed above was that required to neutralize the primary electron beam. However, it is possible for the ion concentration greatly to exceed this value. If the ions are formed in the bombardment region at a rate faster than they can escape, their concentration will increase until conditions for a steady state are met. It is unlikely that a positive space charge density would ensue, since slow secondary electrons would be drawn in to give a neutral plasma.

The positive ions would be mainly D_2^+ produced in the reaction

$$D_2+e\rightarrow D_2^++e'+e'', \qquad \text{(III.8)}$$

which has a threshold[16] at 15.4 ev. The cross section[17] for ionization increases rapidly with bombarding energy to a value of 1×10^{-16} cm^2 at 66 ev. We have already assumed that these ions have a velocity of 10^5 cm/sec.

A D_2^+ ion of this speed, moving at right angles to a magnetic field of 200 gauss, has a radius of curvature of 0.21 cm. Hence, to an appreciable extent, the ions will be constrained by the magnetic field to remain near to the region occupied by the primary electron beam. The mean free path of D_2 at 10^{-2} mm pressure is about 0.85 cm, so some diffusion of ions at right angles to the beam could occur.

Even if the effects of the magnetic field and collisions are neglected there may be an increased ion concentration in and around the electron beam. The number of ions formed per unit volume per second is

$$g=J\sigma_i N(D_2), \qquad \text{(III.9)}$$

where J is the number of primary electrons per second per unit area, σ_i is the cross section of D_2 (or H_2) for ionization and $N(D_2)$ is the number of molecules per unit volume. We take[17] $\sigma_i=0.3\times10^{-6}$ cm^2 (at 21 ev), $N(D_2)=3.54\times10^{14}$ cm^{-3} (10^{-2} mm Hg) and the previously assumed electron flux density $J=7.9\times10^{15}$ cm^{-2} sec^{-1}, and find $g=8.4\times10^{13}$ ions/cm^3/sec throughout the cylindrical electron beam of radius a. The ion concentration at a point $\mathbf{r}$ is given by

$$N_i(\mathbf{r})=(g/4\pi v_i)\int\int\int|\mathbf{r}-\mathbf{r}'|^{-2}d\mathbf{r}', \qquad \text{(III.10)}$$

where the integration is extended over a cylinder of radius a. For $\mathbf{r}$ at the center of the beam, the integrations are easily performed, and one finds

$$N_i(0)=(\pi/2)(ga/v_i)=2.1\times10^8 \text{ ions/cm}^3. \qquad \text{(III.11)}$$

This ion concentration would give a rate of 8×10^5 sec^{-1} for the transition from the α sublevel of $3\,^2S_{\frac{1}{2}}$ to the $3P$ levels. Despite the roughness of this estimate, it would seem quite plausible that the high pressure quenching of the α state discussed in Sec. 8(e) could be attributed to positive ions.

Transitions from the β state to $3P$ will be given by similar expressions to those used above for α, but the rate will be somewhat larger because ω' is smaller. A special consideration is needed at the βe and βf crossing points. Here a frequency $\omega'=0$, and the integration over b in Eq. (III.5) diverges. This divergence arises from the neglect of multiple collisions and radiative decay of the $n=3$ levels. For our problem (ion density $<10^9$ cm^{-3}), the damping effect dominates. It can be shown that a rough, but adequate, way to allow for the damping is to cut off the integration (III.5) at $r=v/\gamma_p$. Numerically one has $v/\gamma_p=5.4\times10^{-3}$ cm, and the cross section is given by Eqs. (III.6) with γ_p replacing ω'. The corresponding W_i' for the β state near crossing points is about the same as the previous $W_i'+W_i''$ for the α state. It is possible that the unexpected nonresonant behavior of quenching near the βf crossing shown in Fig. 14(b) is due to ionic effects.

The cross sections for ionic quenching of the $4\,^2S_{\frac{1}{2}}$ states will be even larger than those for $3\,^2S_{\frac{1}{2}}$. The main effect will be an increase by a factor 3.3 due to a larger matrix element. A weak static or motional electric field produces 6.7 times faster quenching for $4\,^2S_{\frac{1}{2}}$ than for $3\,^2S_{\frac{1}{2}}$.

[16] W. Bleakney, Phys. Rev. **40**, 496 (1932).
[17] J. T. Tate and P. T. Smith, Phys. Rev. **39**, 270 (1932).